Pitfalls and Refinement of 2D Cross-hole Electrical Resistivity Tomography

Haoran Wang[1], Chih-Ping Lin[2]，Hsin-Chang Liu[3]

Abstract: As the conventional surface ERT method is limited by its low resolution at depth, cross-hole electrical resistivity tomography (CHERT) method is increasingly used in the field of geo-environment and hydrogeology whenever possible. Researches regarding CHERT configurations and some negative effects in this method have been useful in survey planning and data interpretation. Nevertheless, some issues remained to be resolved before a standard guideline can be drawn up for conducting CHERT. The symmetric effect was recently pointed out as a major issue in resistivity tomography involving borehole measurements including both borehole-to-surface and cross-hole methods. Symmetrical artifacts emerge for certain types of electrode configuration, which are often desired for better resolution. In this study, the symmetric effect was further investigated in a general two-hole CHERT layout, which is more frequently used in the field. The influence of symmetric effect is found to manifest when the assumption of boundary condition in the inversion is incorrect. The effect of electrode configuration and inversion scheme was further examined and the extended inversion model was found to be more suitable for CHERT data inversion. In particular, the optimal extended range outside the boreholes on each side was shown to be 0.25 times the borehole depth. To mitigate the symmetric effect, a more practical optimal array was proposed. These new suggestions were further verified by a field example.

Keywords: cross-hole ERT, symmetric effect, inversion range

[1]Agrosphere (IBG-3), Institute for Bio- and Geoscience, Forschungszentrum Jülich GmbH, Jülich, Germany.
[2]Professor, National Chiao Tung University, 1001 Ta-Hsueh Road, Hsinchu, Taiwan. E-mail: cplin@mail.nctu.edu.tw; Phone: +886-3-513-1574 (**corresponding author**);
[3] Assistant researcher, National Chiao Tung University, 1001 Ta-Hsueh Road, Hsinchu, Taiwan.

1. Introduction

As a widely used geophysical method, electrical resistivity tomography (ERT) technique has been successfully applied in various fields (Chambers et al., 2006; Wilson et al., 2006; Tsokas et al., 2008). Especially in hydrogeophysics, there have been a large number of studies and applications, such as finding groundwater (Saad et al., 2012), estimating hydrogeological parameters (Brunet et al., 2010), monitoring hydraulic process (Coscia et al., 2011, 2012), and characterization of groundwater contamination (Chambers et al., 2010).

In an ERT survey, the conventional 2D surface ERT method is usually the first choice since it is nondestructive and low-cost. However, the investigation depth of surface ERT is limited to around 1/5 of the length of survey line for a four-pole array (Roy et al., 1971). Furthermore, the resolution of surface ERT decreases rapidly with the increasing depth due to mesh discretization and more importantly the sensitivity distribution (Oldenburg et al., 1999; Friedel, 2003). Cross-hole electrical resistivity tomography (CHERT) method can provide higher resolution at depth at the cost of drilling boreholes (Perri et al., 2012). When conducting CHERT survey, however, conventional surface ERT arrays (e.g., Pole-Dipole, Dipole-Dipole and Wenner-Schlumberger) cannot be directly applied. Accordingly, much progress has been made on optimizing CHERT configurations. Zhou et al. (2000) studied various types of CHERT configuration and revealed the advantages of using AM-N, AM-B, and especially AM-BN arrays. Goes et al. (2004) pointed out the cross-hole tripole-pole configuration is suited for locating small, high-resistivity anomalies between boreholes. Furthermore, 2D and 3D optimized CHERT arrays not confined to a certain configuration type and based on the enhancement of model resolution or sensitivity have also been developed to achieve better CHERT performance (Wilkinson et al., 2006a; Hagrey, 2012; Loke et al., 2014). Undoubtedly, the CHERT method has advanced significantly and many

successful applications in the field of environmental, geotechnical and hydrological engineering have been reported (Slater et al., 2000; Ha et al., 2010; Coscia et al., 2011).

The CHERT method could be a better choice to achieve deeper investigation and higher resolution if boreholes are available. However, many influence factors in the CHERT survey, such as borehole deviation, borehole diameter and filling, electrode size, and shadow effect have been identified (Nimmer et al., 2008; Yi et al., 2009; Rücker et al., 2011; Leontarakis et al., 2012; Wagner et al., 2012). The undesirable effects caused by these factors and their countermeasures have been investigated. Nevertheless, there are still some problems that have been overlooked and could have adverse effects on CHERT results. The symmetric shadow effect is a major problem in ERT involving borehole measurements. This phenomenon caused by certain types of electrode configuration and its consequence of possibly misinterpreting the anomaly distribution drew some research attention more recently (Tsourlos et al., 2011, Bellmunt et al., 2016; Wang and Lin, 2018). Tsourlos et al. (2011) revealed this effect and pointed out its possible cause in the setting of 2D borehole-to-surface ERT (BSERT). Wang and Lin (2018) further clarified the root cause of symmetric effect being the coexistence of current pole and potential pole in the same borehole, and proposed countermeasures to suppress the symmetric effect in borehole-to-surface ERT (BSERT). Bellmunt et al. (2016) investigated the same problem in three-hole 2D CHERT and proposed two indices, In-panel/Off-panel Sensitivity (IOS) and Anomaly Detection (AD), to evaluate different arrays. An organized way to select the most adequate electrode combinations was proposed based on IOS, AD, and geometric factor (***K***) in the context of resolving and monitoring plume migration. Many thresholds (i.e., AD, IOS, and ***K***) for data selection are involved, and they were referenced qualitatively without quantitative criterion. More importantly, the indices AD and IOS are model-dependent (i.e., function of resistivity distribution and cross-

hole layout) and can only be calculated in a three-hole system. The analyses of geometric factor as a function of electrode separations are useful to avoid sharp changes in $\boldsymbol{K}$, but this measure may not be sufficient to ensure data quality as there may still exist a certain amount of high $\boldsymbol{K}$ data in the dataset. Furthermore, the 2D CHERT survey is probably more often conducted with only two boreholes. The symmetric effect and its effective countermeasure in a two-hole cross-hole ERT for general survey purpose need further investigation.

In CHERT, the effect of resistivity structure outside the CHERT panel(s) is another issue. Shima. (1989) discussed the effect of surrounding resistivity structures in a closed square survey layout using pole-pole array and suggested that the area outside the target zone should also be analyzed. The inversion of CHERT data usually focuses on the major area of interest between the two boreholes. There is no clear instruction regarding how to deal with the area outside boreholes. Daily et al. (1991) suggested that it is better to extend the inversion region first to check the outside anomaly. If no anomalous structures are evident beyond the boreholes, a more limited area bounded between boreholes can be used, which may result in the highest possible spatial resolution for the region of interest. However, such a straightforward approach may not be effective in complex heterogeneous field conditions. Anomaly located outside the interested area may affect the reconstruction of the image between boreholes, and in turn, the outside region may also be influenced by the targeted anomaly between boreholes.

It should be pointed out that the influence of outside anomaly actually comes from two aspects. One is the symmetric effect caused by some certain electrode configurations and the other is the incorrect setup of boundary conditions in the inversion model. Under these two effects, it is necessary to explore the influence of outside anomaly on two-hole CHERT survey. In this study, several widely used CHERT arrays were investigated in this aspect. For practical consideration,

general suggestions on the selection of CHERT array and the size of extended inversion model were provided based on the analyses of geometric factor and absolute sensitivity profile. A field case was also shown to compare the results of different arrays and data processing schemes.

2. Numerical modeling

To investigate the influence of outside anomaly in two-hole CHERT, full 3D forward modeling by COMSOL Multiphysics® was adopted to generate synthetic dataset of different array types. It has already been shown that the computation for the classical ERT forward problem in COMSOL Multiphysics® is accurate and comparable with the analytical solution (COMSOL, 2015). The electrical potential is obtained by solving the following Poisson's equation:

$$\nabla \cdot (-\sigma \nabla \varphi) = -I \cdot (\delta(r - r_A) - \delta(r - r_B)) \quad (1)$$

where σ is the electrical conductivity of the medium, φ is the electrical potential, I is the electrical current, and $\delta(r - r_A)$ and $\delta(r - r_B)$ are the Dirac delta function for a point source located at position r_A and r_B respectively. The air layer over the model surface is considered as electrical insulation, and the electrical flux normal to the surface is null. As the distance from the point source increases, the potential decreases and approaches asymptotically to 0. Thin infinite layers were placed at the surrounding and bottom boundaries of the 3D model and the boundary condition of φ =0 was used for these boundaries by setting their outer faces connected to electrical ground. The discretization method used in the forward calculation is the same as what was presented in Rücker et al. (2006). Model elements are refined around the electrodes and on the anomaly bodies. Global meshes are gradually increased in size with increasing distance from the electrodes. The 3D finite element method was used to ensure the synthetic data is more realistic as the mesh is more refined and the electrodes are point electrodes as in the field survey. The synthetic model and CHERT arrays used in this study are described next.

2.1. Synthetic model

Bellmunt et al. (2016) investigated the capability of different CHERT configurations to resolve the plume migration direction in a three-hole system with special consideration of the symmetric effect. To enable comparative discussion, similar synthetic models were adopted in this study but in a two-hole CHERT setup. As shown in Figure 1, the synthetic model has two boreholes 10 m apart with 21 electrodes in each. The electrode spacing in each borehole is 1 m. The moving plume is simulated using three square bodies with side length twice the electrode spacing. The center of the anomaly is located at 10 m below the ground surface, and 1 m, 3 m and 5 m horizontally away from the borehole for stages A, B, and C, respectively. The resistivity of the anomaly is 10 Ωm while the background resistivity is 100 Ωm. The three different stages of plume migration were used in this study to investigate the influence of outside anomaly located at different distances from the borehole.

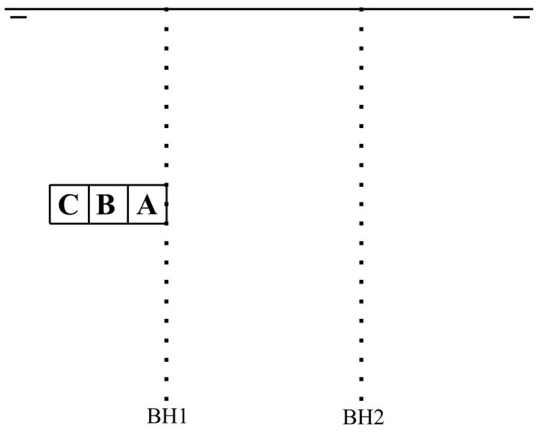

Figure 1. Schematic of the synthetic model

2.2. CHERT arrays

One consideration of the outside anomaly is for the symmetric effect, which has been more thoroughly discussed in Tsourlos et al. (2011) and Wang and Lin (2018) in the borehole-to-surface layout. The symmetric effect is an undesirable effect that produces mirrored artifact opposite to the target anomaly with the borehole being the symmetric axis. Besides the borehole-to-surface method, the symmetric effect was also found in the cross-hole method (Bellmunt et al., 2016). In the case of BSERT, Wang and Lin (2018) revealed the root cause of symmetric effect to be coexistence of current electrode and potential electrode. According to the results in Bellmunt et al. (2016) and our additional simulations, this is also true for CHERT. Electrode configurations in which one current pole and one potential pole exist in the same borehole concurrently (e.g., A-BMN/AMN-B) will induce symmetric effect but have higher resolution. On the other hand, electrode configurations with potential poles in one borehole and current poles in the other (e.g., AB-MN) have no symmetric effect but exhibit lower spatial resolution.

For a specific fluid and gas plume migration problem, Bellmunt et al. (2016) proposed two indices, the In-panel/Off-panel Sensitivity (IOS) for evaluating the capability of resolving direction and the Anomaly Detection (AD) for assessing the anomaly detection ability. A group of reduced and optimized electrode arrays (OPT) based on these two indices were then selected. However, the two indices IOS and AD depend on both the resistivity model and cross-hole layout, which means the OPT array is problem specific and not applicable to general surveys.

To designate the type of electrode array, we use the common notations in which A and B represent the current electrodes, and M and N represent the potential ones. The position of the electrodes in two boreholes are designated by two groups of capital letters (i.e., AB-MN means that A and B are located in one borehole while M and N are located in the other one). Electrode arrays investigated in this study include the same three arrays discussed in Bellmunt et al. (2016),

AB-MN, A-BMN/AMN-B (abbreviated as TP in this paper) and the optimized array (OPT, this is possible because the same resistivity model and borehole layout were used). Since AM-BN array was not favoured in Bellmunt et al. (2016) according to the AD and IOS indices, this study tested another commonly-used Bipole-Bipole (abbreviated as BB) array, which comprises AM-BN and pure in-hole data with four electrodes in the same borehole (AGI, 2014). The resultant amount of data for AB-MN, TP, OPT, and BB arrays were 2870, 1540, 518, and 1664, respectively.

3. Results and discussions

To simulate the field measurements, the ideal model response was contaminated by adding a noise, Δd, following Bellmunt et al. (2016):

$$\Delta d = d\delta + \chi \quad (2)$$

where d is the noise-free response, and δ and χ are random numbers. The δ is normally distributed with zero mean and standard deviation σ, and χ is uniformly distributed in the interval $[-\varepsilon, +\varepsilon]$. These two random numbers (δ, χ) emulate the relative accuracy (δ) of the field data, and the instrumental resolution (χ). Values of 0.015 for σ and 10^{-4} V/A for ε were used. The synthetic data was inverted for resistivity section using the robust model inversion (Loke et al., 2003; Loke 2016) of RES2DINV software as in Bellmunt et al. (2016). The mesh used in the inversion was regular square with the side length the same as electrode spacing.

3.1 Results of confined inversion model

In Figure 2, data of different electrode arrays and earth models were inverted using typical confined model between two boreholes. The three columns represent the results of anomaly located at stage A, B and C respectively, and the four rows represent different arrays. It can be seen from all results that the homogeneous resistivity model between the two boreholes was not recovered. There are some extremely high and low resistivity values appeared in the inverted sections,

especially when the anomaly is located close to the borehole. And the symmetric effect can also be observed in the results of BB, TP, and even OPT array. This was found to be caused by the off-panel anomaly when using the confined model for inversion. The erroneous results can be attributed to the fact that the sensitivity distribution outside the boreholes is also considerable and the outside anomaly significantly affects the measured potentials. Furthermore, in the model confined between the two boreholes, the region outside the boreholes is handled by infinite element domain. Treating the off-panel elements by infinite boundary condition is not a robust inversion strategy because the off-panel elements are also unknowns and play a significant role in the measured potentials. This incorrect assumption results in apparently incorrect solution when the resistivity values in the region outside the boreholes are heterogeneous and different from the boundary condition imposed. The above observations and discussion imply that, in general, it is necessary to extend the inversion model. To determine the required extended range for the inversion model, sensitivity distributions of different arrays were examined next.

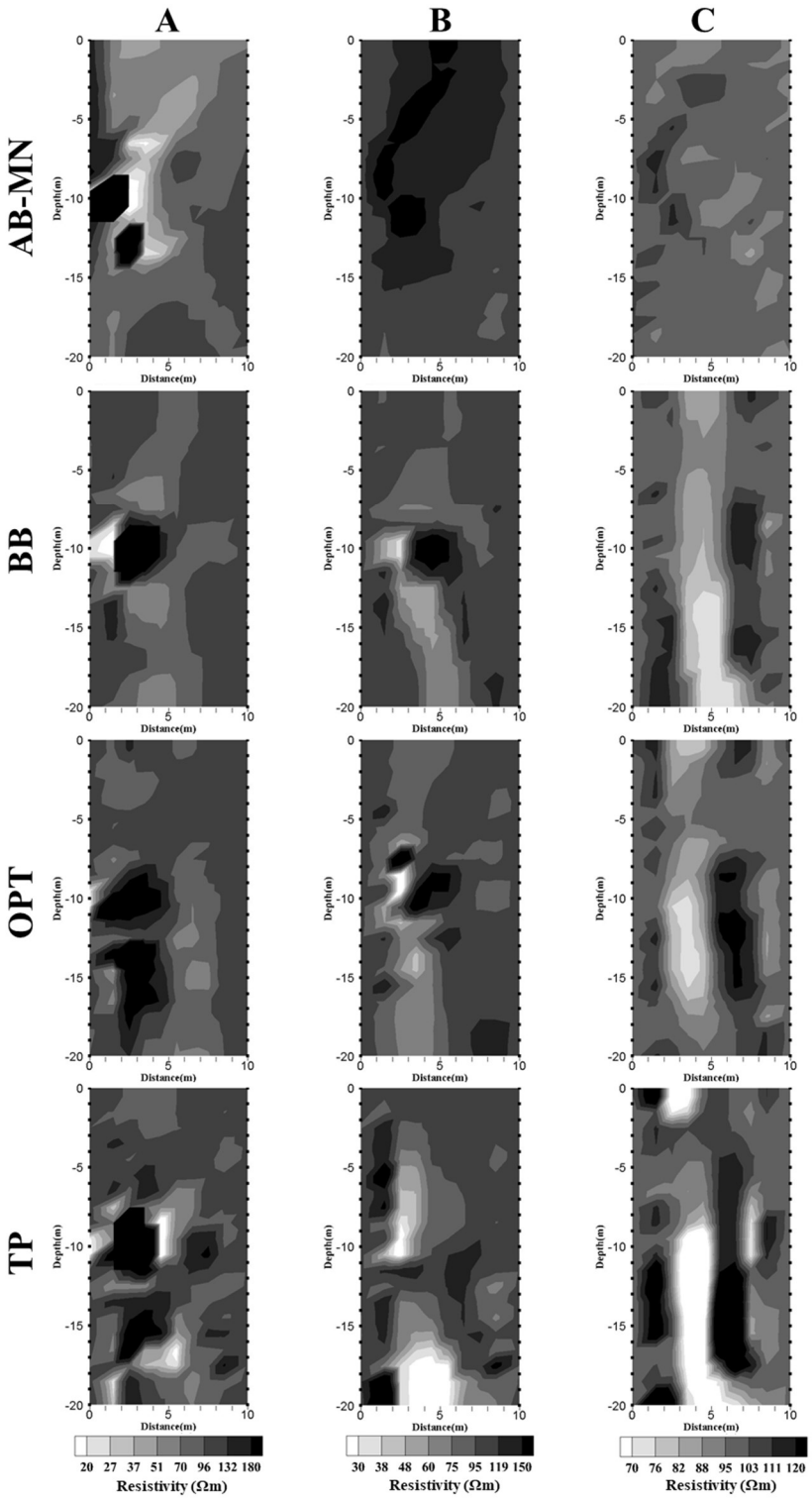

Figure 2: Inversion results of different electrode arrays and earth models using typical confined inversion model

3.2 Sensitivity distribution of different CHERT arrays

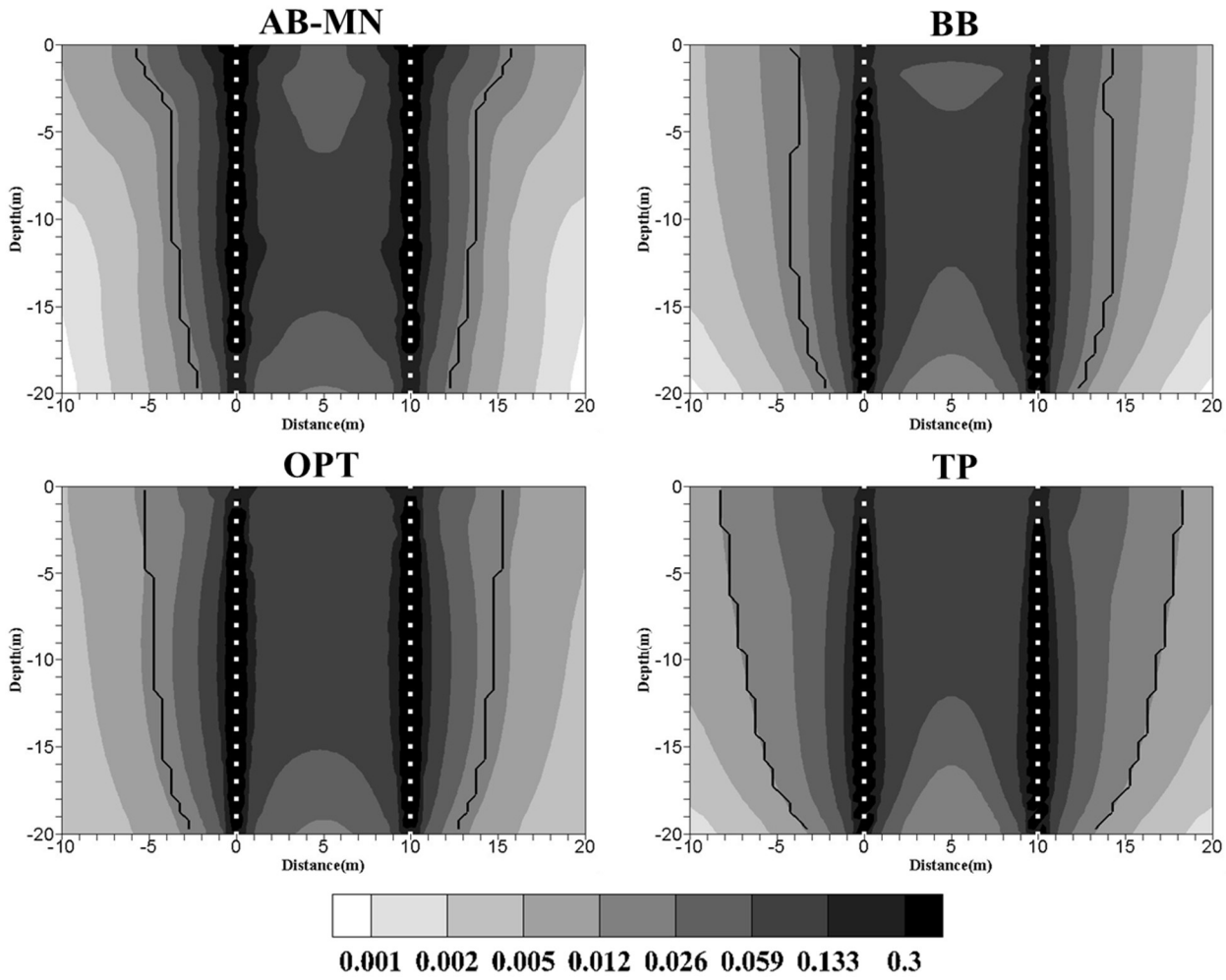

Figure 3: Normalized sensitivity distribution of different arrays

The sensitivity distribution of an ERT array discloses the degree to which a change of resistivity in each area would influence the potential measured by the array. The higher the sensitivity value, the greater is the influence of the subsurface region on the measurement. The sensitivity distribution profile of a group of arrays is the sum of absolute values of all sensitivity patterns and indicates the capability of reconstructing the subsurface and its effective influence

range. Sensitivity of a pole-pole array can be calculated by the following function (Park and Van., 1991):

$$\frac{\delta\varphi}{\delta\rho} = \int_V J \cdot J' \, d\tau \tag{3}$$

where J is the current density from a point source at the transmitter (current pole), J' is the current density from a point source at the receiver (potential pole) and $d\tau$ represents a small volume element. For a four-pole electrode array, the sensitivity function can be written as:

$$\frac{\delta\varphi}{\delta\rho} = \int_V (J_A \cdot J_M - J_A \cdot J_N - J_B \cdot J_M + J_B \cdot J_N) \, d\tau \tag{4}$$

where *A* and *B* are the positive and negative current poles, *M* and *N* are the positive and negative potential poles respectively.

In this study, sensitivity values of each array are calculated using a homogeneous model of 100 Ωm. It should be noted that the CHERT method is very different from its seismic or radar counterpart, the cross-hole travel time tomography method. The sensitivity distribution of a CHERT survey covers not only between the boreholes but also outside the boreholes. As shown in Figure 3, the sensitivity of CHERT arrays is significant not only in the interested area between two boreholes but also have significant effect outside the boreholes. Therefore, an extended inversion model should be used in the CHERT inversion. However, the number of unknowns and hence the inversion uncertainty increase with increasing extension range. The question here becomes how to determine a reasonable extended range for inversion.

To estimate a reasonable extended range, the lowest sensitivity value between two boreholes of each array type is considered as the threshold of acceptable sensitivity. Sensitivity outside the two boreholes decays with increasing distance from the boreholes and the black lines in Figure 3 indicate the envelope of the sensitivity threshold. It can be seen from Figure 3 that different array types present different sensitivity distribution outside the boreholes. The sensitivity distributions

are all symmetrical except for the BB array. Hence, the external envelope of sensitivity threshold for the BB array are not symmetrical. Of all the array types examined, the region encompassed by the threshold envelopes is the broadest for TP array. Nevertheless, the threshold envelopes of all the four array types are around 5 m away from the boreholes.

3.3 Results of extended inversion model

Based on above analyses, inversions were re-performed with extended models and some results are shown in Figure 4 and 5. We defined the extended ratio (***eR***) as the ratio of extended distance outside the boreholes to the borehole depth. Two extended ratios, ***eR***= 0.125 (Figure 4) and ***eR***= 0.25 (Figure 5) were considered for the first trial, and further discussion about the most suitable extended range is presented in the next session. It can be seen from Figure 4 and Figure 5 that, after using the extended inversion model, the disagreement with the actual homogeneous model between the two boreholes has been reduced, comparing with the results using the confined inversion model in Figure 2. The anomaly located outside boreholes can also be reconstructed by extending the inversion model.

When the anomaly is located at stage A, both Figure 4 and 5 show that the external anomaly can be well recovered by all array types. However, the results of AB-MN array show more heterogeneity between the two boreholes with some extremely high resistivity areas. As the anomaly moves to stage B, Figure 4 shows that the extended model with ***eR***=0.125 does not cover the complete area of anomaly and is not sufficiently extended according to the sensitivity study in the previous section**.** As a consequence, the symmetric effect appears in the results of TP, BB, and even OPT arrays. Similarly, artefacts as a result of insufficient model extension can also be observed in the results of stage C in Figure 4. Results of AB-MN array do not have symmetric effect, but the external anomaly at stage B and C are not well resolved.

Inversion of the same dataset but using different extended inversion model produces considerably different results. Apart from those arrays that can induce symmetric effect intrinsically, such as TP and BB, the OPT array can also introduce some symmetric effect if the cross-hole inversion does not include sufficient external extension range, as shown in Figure 4. When the inversion model space is extended to ***eR***=0.25 to cover all three stages of anomaly and all the sensitive region under this cross-hole layout, Figure 5 shows that, in spite of the symmetric effect, anomalies located at stage A and B are clearly reconstructed in the results of all arrays. The anomaly at stage C can also be approximately captured by TP or OPT array. Furthermore, comparing with the results in Figure 4, the symmetric effect is also greatly reduced by further extending the inversion range.

Figure 5 shows that there are still some symmetric effect in the result of TP array and BB array even though larger extended inversion model has been used. These two arrays are not completely immune to the symmetric effect because current electrode and potential electrode coexist in the same borehole. The BB array (used in this study and commonly seen in engineering practice because of the commercial software) actually contains AM-BN configuration (illustrated in Bellmunt et al., 2016) and pure in-hole configuration (four poles in one borehole) which can induce severe symmetric effect (Wang and Lin, 2018) because the sensitivity pattern of which is completely symmetric. On the other hand, the OPT array in the two-hole layout does show its capability to suppress the symmetric effect while maintaining good resolution.

If we examine the root mean square (RMS) value of the data fit error, results of AB-MN array with confined inversion model have very high RMS value over 15%. Being an array type that does not exhibit the symmetric effect, it is difficult to find a model constrained between the two boreholes to fit the measured data well with the incorrect boundary condition, hence resulting in

high RMS. However, results of other arrays with confined inversion model have much lower RMS value (range from 3% to 6%), because of the symmetric effect and non-uniqueness in the inversion. Reconstructed model with anomaly located at the symmetrical area can fit the data very well for arrays with the symmetric effect.

Two major points can be drawn from the above discussions: (1) the extended inversion model is generally more correct and strongly recommended for processing CHERT data; (2) the OPT array has great potential in providing good imaging fidelity while suppressing the symmetric effect. However, there are still some problems in exercising each of two major points: (1) Considering the variety of CHERT surveys (e.g., different borehole depth, borehole separation, and choice of electrode array), a general guideline for deciding the extension range of inversion model is yet to be proposed; (2) Instead of selecting arrays based on AD and IOS, an alternative and more practical selection scheme is desired without having to assume certain a priori resistivity model.

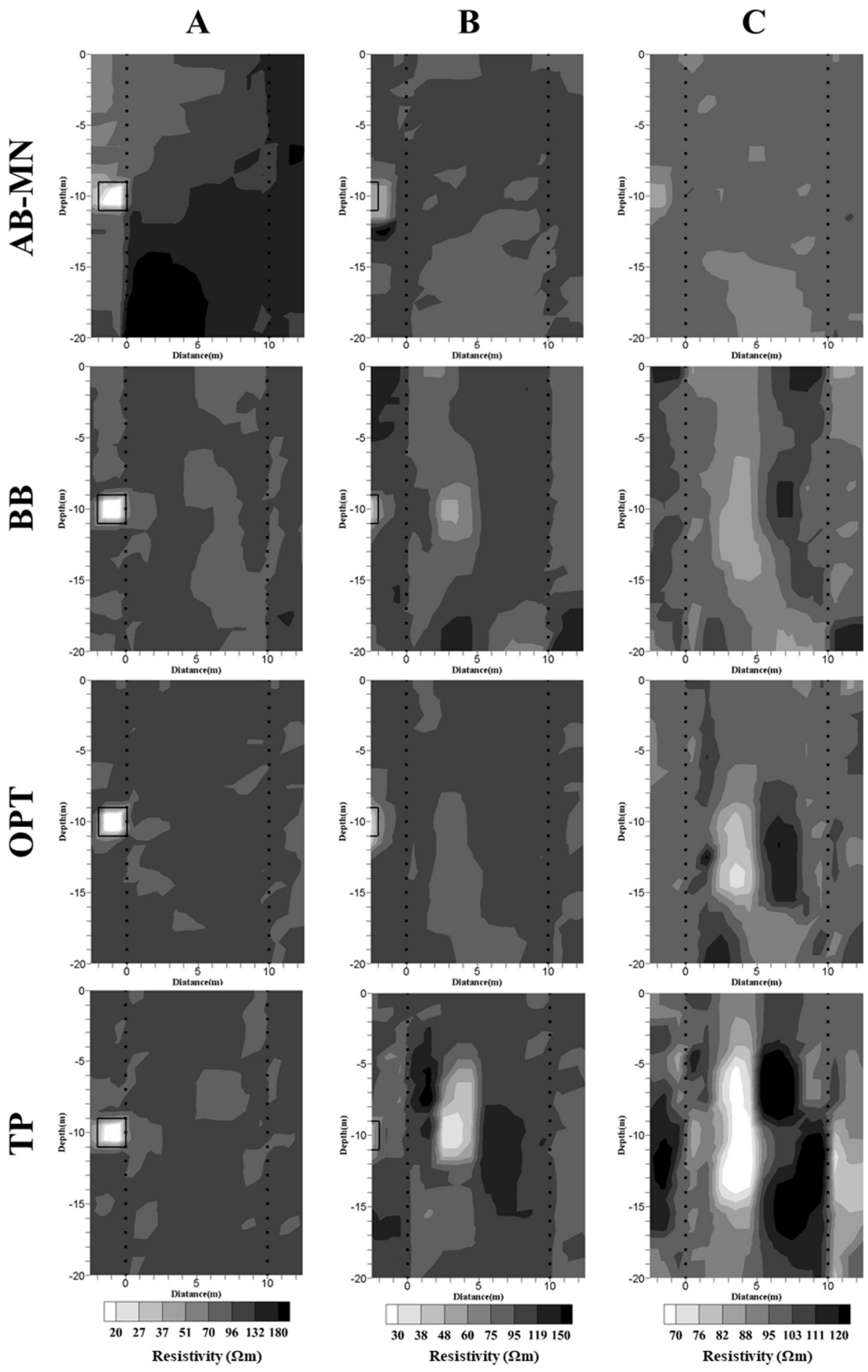

Figure 4: Inversion results of different arrays and earth models for ***eR***=0.125

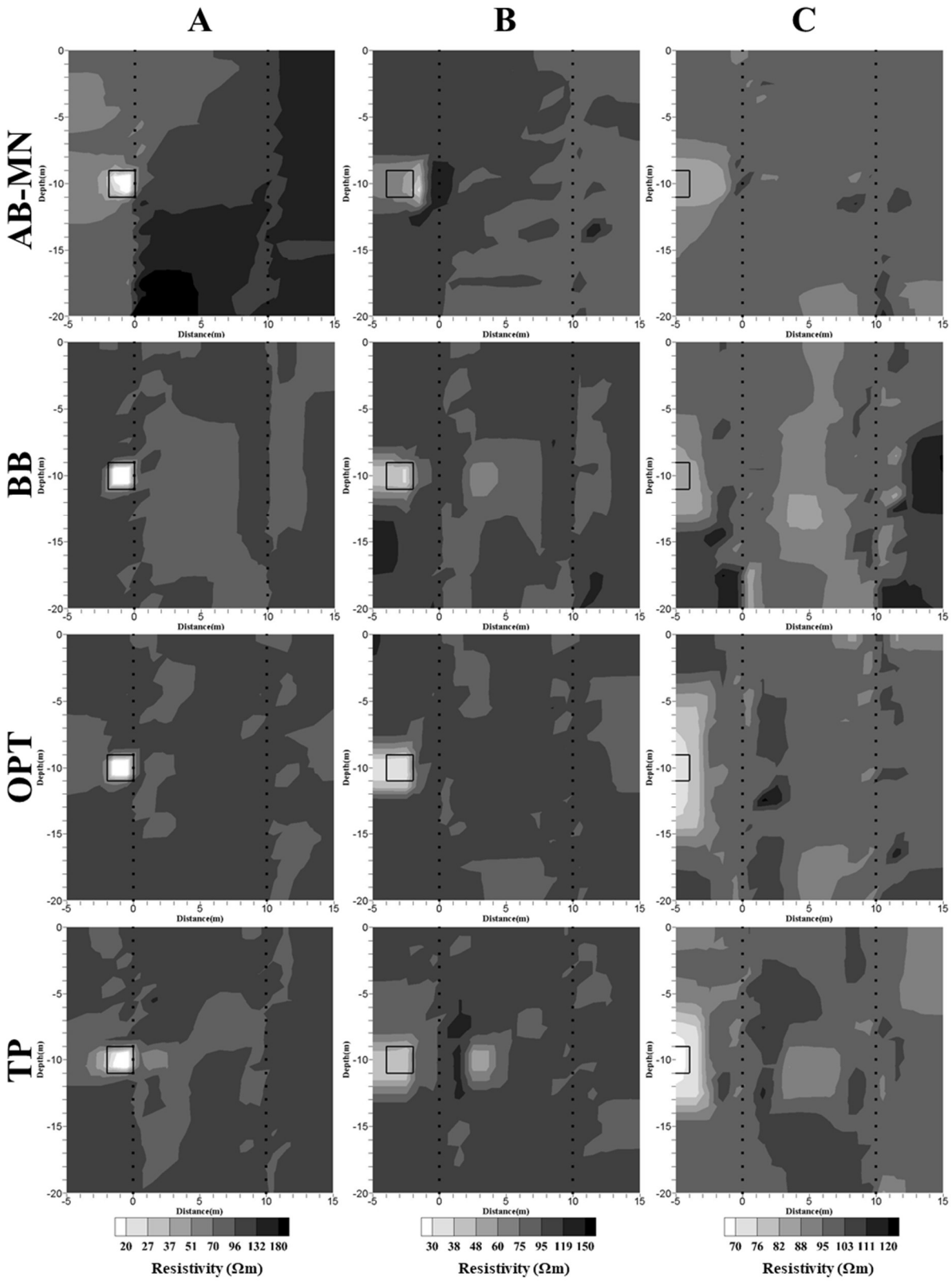

Figure 5: Inversion results of different arrays and earth models for ***eR***=0.25

4. Practical considerations

4.1 Geometric factor

Voltage is the response data measured in the ERT method. For each measurement, an apparent resistivity can be calculated using the following equation:

$$\rho_a = K\frac{V}{I} \tag{5}$$

where ρ_a is the apparent resistivity, V and I are the measured voltage and injected current respectively, and K is the geometric factor which depends on the spatial arrangement of the four electrodes (Loke, 2016). Calculation method for the geometric factor of CHERT array has been reported in Guo et al. (2014). From Equation (5), it can be seen that larger geometric factor will result in lower voltage reading, which becomes more sensitive to noise. Hence, it is necessary to consider geometric factor as a data filter to ensure good quality of field data. K values for AB-MN, TP and OPT arrays were calculated and the histograms are presented in Figure 6.

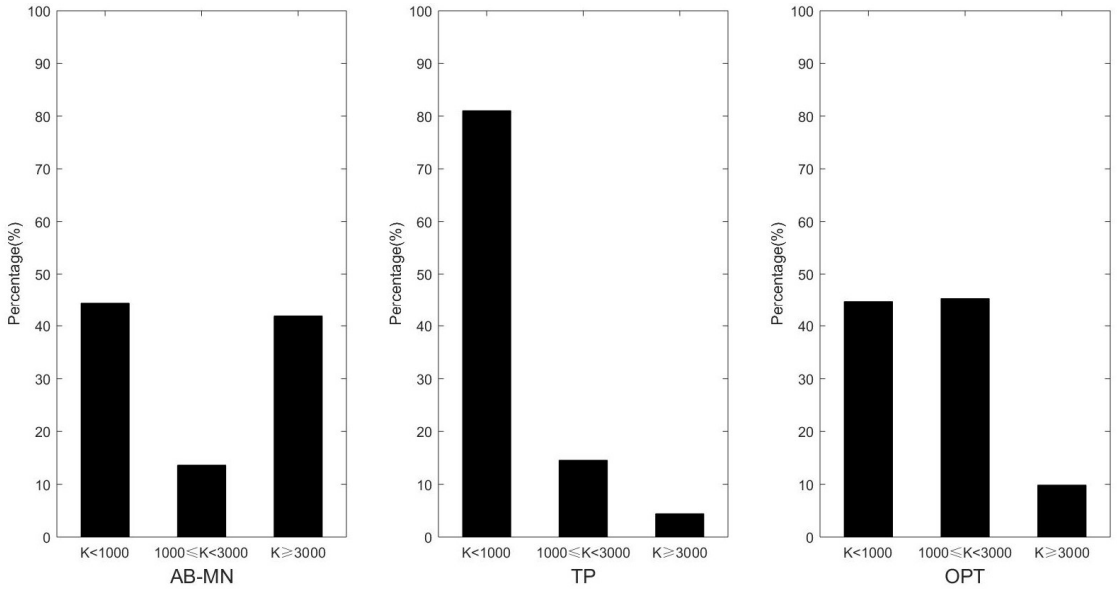

Figure 6: Geometric factor statistics of different arrays

In the resolution-based optimized ERT array method (Loke et al., 2010), ***K*** value of the dipole–dipole array with maximum dipole separation n=6 and the current/potential dipole length a=1 (***K*** ≈1055) was considered as the threshold for ***K*** value filter. Figure 6 shows that both the AB-MN and OPT arrays have over 50% of data with ***K*** value greater than 1000, while TP array has around 80% of data with ***K*** value under 1000. These results indicate that, even if the sharp change of geometric factors is avoided, there may still exist some amount of high ***K*** data that are more susceptible to noise contamination in the field. Therefore, we propose to apply a general ***K*** threshold, which can ensure data quality and also avoid the sharp ***K*** increase (as suggested in Bellmunt et al. (2016)) at the same time. As described in the previous section, there are totally 2870 and 1540 data points for AB-MN and TP configuration respectively. The ***K*** threshold value of 900 was applied to remove those arrays with large geometric factor, reducing the data to 1226 and 1224 points for AB-MN and TP configuration, respectively. While the ***K*** threshold value may be adjusted by choice, the threshold value around 1000 is recommended to adequately ensure good quality data in most ERT cases.

4.2 Combined array type for CHERT survey

The suggested optimal array proposed by Bellmunt et al. (2016) was based on the concept of combined data inversion of the AB-MN and TP configurations. Selection of the optimized dataset was based on two indices, In-panel/Off-panel Sensitivity (IOS) and Anomaly Detection (AD). These two indices are model dependent and not available for general practice of CHERT survey. In light of this, a more general data selection method is proposed regardless of field condition and cross-hole layout. Understanding the distinct characteristics of AB-MN and TP arrays in symmetric effect and resolution, the selection scheme is to reach a good compromise between the symmetric effect and resolution. After applying the ***K*** filter, there are 1226 and 1224 data points

remaining for AB-MN and TP configuration respectively. We first combined all data points for the inversion and then reduced a fraction of data for AB-MN or TP array by skipping MN separations. Different ratios (1:4, 1:3, 1:2, 1:1, 2:1) of AB-MN to TP data amount were tested. For ratios 1:4, 1:3, 1:2, and 1:1, all results are similar and only the case of 1:2 is presented in Figure 7. Comparing to the results of OPT array in Figure 5 in terms of model resolution and restraining the symmetric effect, similar satisfactory results were obtained by these data combination ratios. The results show that sufficient TP data is desirable to enhance model resolution, but some fraction of AB-MN is needed to effectively suppress the symmetric effect. The best data ratio is no doubt model dependent as some resistivity models are less or more asymmetrical with respect to boreholes than others. The data combination with 1:2 AB-MN/TP ratio after the $\boldsymbol{K}$ filter was adopted as a general or nominal optimized array (NOPT) for the following considerations. The symmetric effect may manifest when there is too much TP data in the combined dataset, as also observed in the combined data inversion of borehole-to-surface survey (Wang and Lin, 2018). A ratio of 1:2 provides sufficient AB-MN data for cases where symmetric effect is critical. On the other hand, it is possible to further lower the ratio to 1:3 or 1:4 from the 1:2 dataset if so desired for cases where symmetric effect is not a concern (e.g., the resistivity is quite uniform in horizontal direction). The suitability of this ratio is also validated by the following field example. Although the OPT array has fewer data points for time efficiency, the proposed NOPT array is particularly advantageous to field data quality control and easy implementation independent of resistivity model and cross-hole layout. The data amount may be further reduced but keeping the same ratio for time efficiency. However, detailed investigation into dynamic monitoring is beyond the scope of this study.

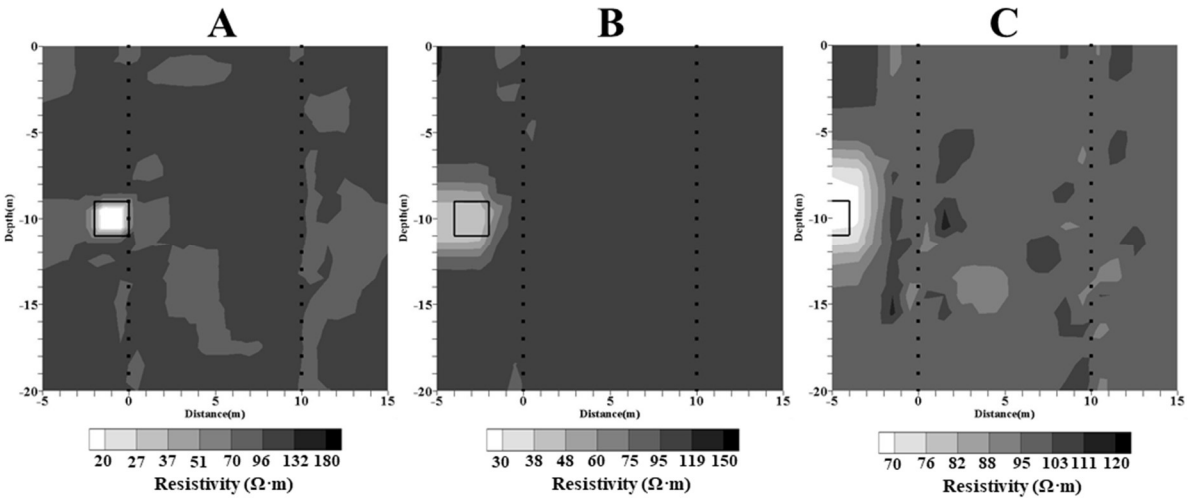

Figure 7: Inversion results of NOPT array for the three stages of anomaly (***eR***=0.25)

To further compare the tomographic capabilities of the OPT and NOPT arrays, the model resolution, which stemmed from linear inverse problem and is now widely adopted in ERT optimization and model appraisal (Stummer et al., 2004; Loke et al., 2010; Wilkinson et al., 2006b; Wagner et al., 2015), was calculated using the following equation:

$$\boldsymbol{R} = (\boldsymbol{S}^{\boldsymbol{T}}\boldsymbol{S} + \boldsymbol{\lambda C})^{-\mathbf{1}}\boldsymbol{S}^{\boldsymbol{T}}\boldsymbol{S} \tag{6}$$

where $\boldsymbol{R}$ is the resolution matrix, $\boldsymbol{S}$ is the sensitivity or Jacobian matrix, which can be calculated by Eq. (4) for four-pole arrays, $\boldsymbol{\lambda}$ is the damping factor, and $\boldsymbol{C}$ is the roughness matrix. As applied in the ERT array optimization (Wilkinson et al., 2006b), a damping factor of $\boldsymbol{\lambda} = 2.5 \times 10^{-6}$ and identity matrix for the roughness matrix were used in the calculation. Diagonal elements of resolution matrix are presented in Figure 8, showing the two arrays have similar resolution distribution, but NOPT array has higher mean value of resolution.

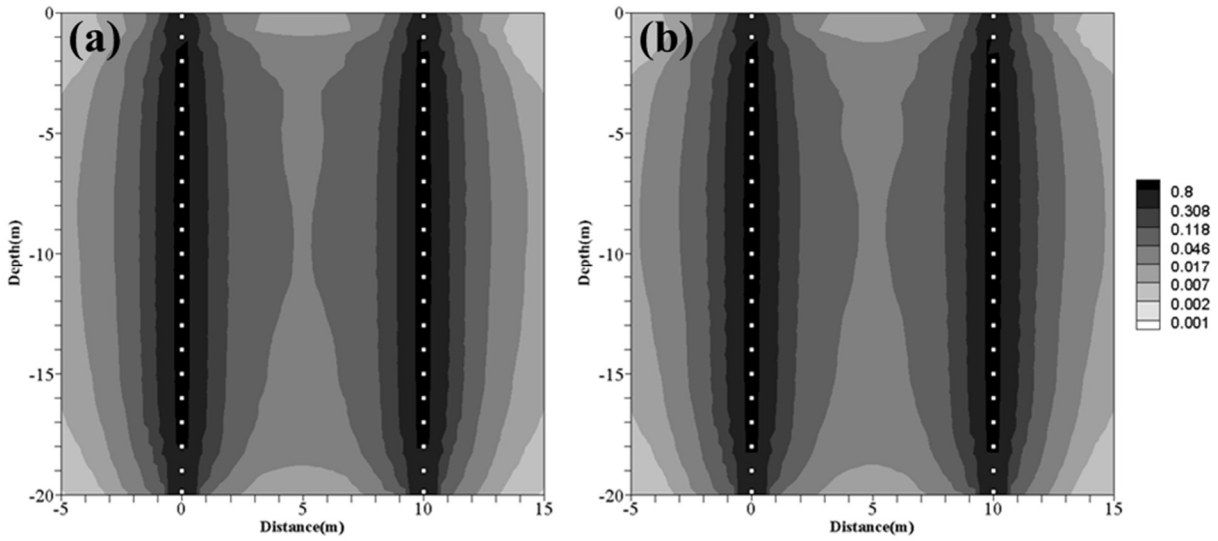

Figure 8: Distribution of model Resolution for (a) OPT and (b) NOPT array

4.3 Relationship between borehole length and extended range

As discussed earlier, the sensitivity outside boreholes has a limited influential range to about 5m away from the borehole in the synthetic model. To confirm this statement and quantify the minimum required extended range, two more synthetic models in which the anomalies are located farther away were performed. In Figure 9, the anomaly is located at x=-7m and z=-10m for Figure 9(a) and 9(b), and x=-9m and z=-10m for Figure 9(c) and 9(d). In this regard, only the results of NOPT array were presented in the figure. Comparing Figure 9(a) with 9(b) and 9(c) with 9(d), there is no significant difference between the results obtained using the same dataset but different extended range in the inversion. Only some minor artifacts are induced. The preset anomalies farther away from the borehole are not reconstructed in Figure 9(b) and 9(d) and do not affect the results in Figure 9(a) and 9(c). This confirms that sensitive region in this layout is limited to about 5m outside the boreholes and the anomaly located beyond this region cannot be detected even if the inversion is extended to cover the anomaly. Extended inversion model with extended ratio of

eR=0.25 seems to be the best choice for this case (borehole depth 20m and borehole separation 10m).

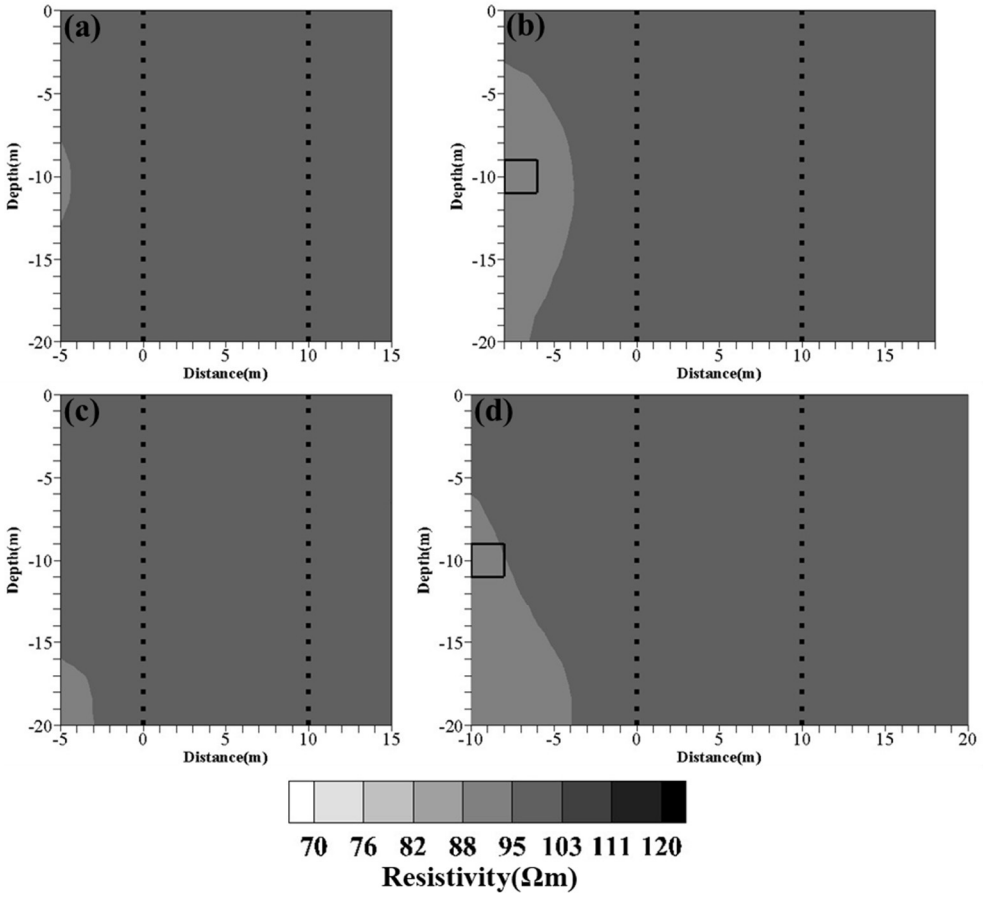

Figure 9: Inversion results for (a) center of anomaly at x=-7m and ***eR***=0.25; (b) center of anomaly at x=-7m and ***eR***=0.4; (c) center of anomaly at x=-9m and ***eR***=0.25; (d) center of anomaly at x=-9m and ***eR***=0.5.

To give a more general suggestion on the extended ratio, sensitivity distributions of different CHERT layouts were calculated to investigate the relationship between borehole depth and the needed extended range. According to previous studies, the borehole spacing was suggested to be 0.5 times the borehole depth, and no more than 0.75 (e.g., LaBrecque et al., 1996). The sensitivity decreases with increasing distance from the borehole on both sides. Hence, the sensitivity of the

center region between the two boreholes is also lower. The restraint of borehole separation is to ensure sufficient sensitivity within the entire region between the two boreholes. Therefore, the borehole spacing was fixed to be half of the borehole depth in the numerical simulations and the electrode spacing was 1m in all cross-hole layouts. Eleven different borehole depths from 10m to 30m were simulated. The array used in this part is also the NOPT array with 1:2 (AB-MN:TP) ratio. To obtain NOPT arrays for different cross-hole layouts, AB-MN and TP arrays were generated first. Arrays with geometric factor over 900 were then removed. To reduce the AB-MN data, the skipped MN were used (e.g. 3, 5, 7…).

Sensitivity distributions were also calculated using a homogeneous model of 100 Ωm. The lowest sensitivity value in the region between the two boreholes was considered as the threshold to determine the lower limit of the sensitivity outside the boreholes at different depths. The lower-limit distances from the borehole at different depths were averaged to determine the required extended ratio. The calculated extended ratio shown in Figure 10 is the ratio of the average lower-limit distance to the borehole depth. It can be seen that the calculated extended ratios are all around 0.25. Current ERT inversion software mostly do not automatically control the CHERT inversion range and the default inversion setting is simply to invert for the region between the two boreholes. According to Figure 10, the general and default inversion range can be set as $\boldsymbol{eR}$=0.25. We also tested the extended ratio calculation on different borehole spacings in the case of 20m borehole depth. The calculated extended ratio is 0.16 for borehole spacing 5m and is 0.257 for borehole spacing 15m. Therefore, as a general suggestion, $\boldsymbol{eR}$=0.25 is reasonable and enough.

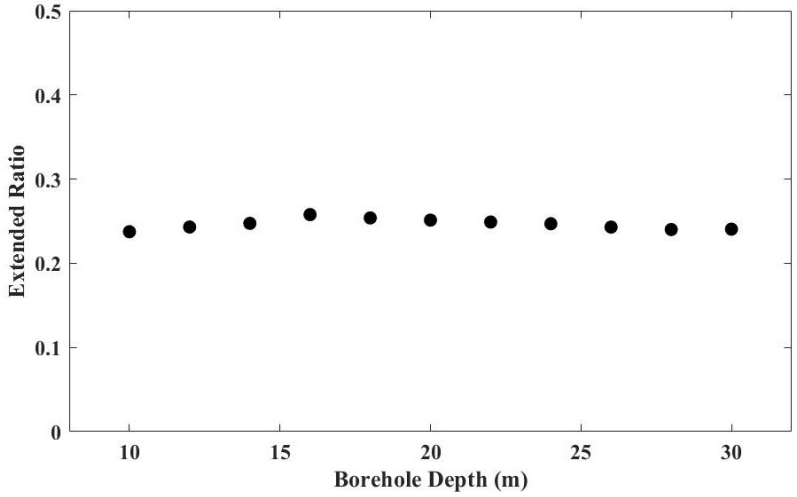

Figure 10: Calculated extended ratio (***eR***) of different borehole depth

5. Field Example

A field experiment was carried out to support the above discussions. The experimental site is located in a motor vehicle factory, where the target area was contaminated by trichloroethylene (TCE). The subsurface condition within the investigated area is mostly gravel with sand. In-situ bioremediation was chosen as the remediation measure, in which low resistivity agents were injected at depths between 5m and 10m using the double packer injection (DPI) method. The injection point is located about 1.5m away from the cross-hole panel. Our CHERT experiment was carried out three months after the injection, therefore the possible resistivity distribution was not clear. The resistivity instrument used for the field work was AGI SuperSting R8. Ring-type borehole electrodes were wrapped around PVC casings at 1 m spacing down to 12m below the ground surface. The electrode contact resistance was too high above the groundwater level at 3m depth, so only 10 electrodes were used from 3m to 12m below the ground surface. The borehole separation is 7m, which results in a borehole separation to depth ratio equal to 0.78 beyond the suggested 0.5 and even slightly above 0.75. Hence, the reciprocal measurement method (Slater et al., 2006) was applied to ensure good data quality and evaluate the capability of AB-MN and TP

arrays in resisting noise. A pair of reciprocal measurements should be identical in theory; however, in reality, the data may be distorted by imperfect electrode contact or filed noise. The reciprocal measurement error in percentage is defined by the following equation:

$$\boldsymbol{e} = 0.5 \times \left(\left| \frac{d_1 - d_2}{d_1} \right| + \left| \frac{d_1 - d_2}{d_2} \right| \right) \times 100\% \quad (7)$$

where $\boldsymbol{e}$ is the error percentage, d_1 and d_2 are the pair of reciprocal data.

Figure 11 presents the statistical bar charts of reciprocal measurement error and geometric factor. In the measured dataset, about 70% of AB-MN data and over 80% of TP data have low reciprocal error under 5%. Unfortunately, AB-MN has more than 50% of electrode arrays with geometric factor greater than 900, which was considered as one of the criteria for selecting resolution-based optimal ERT arrays (Loke et al., 2010). Five percent reciprocal measurement error and 900 for geometric factor were used as the threshold to select the dataset for data inversion. After the data was filtered by $\boldsymbol{K}$ and reciprocal error thresholds, there are 204 TP data points and 95 AB-MN data points. The data was directly used to have 1:2 (AB-MN:TP) data combination. Some MN distances were then skipped to test the performance of other two combination ratios. Ratio 1:1 contains 95 AB-MN and 94 TP data points and ratio 1:4 contains 54 AB-MN and 204 TP data points. A slightly lower $\boldsymbol{eR}$=0.222 was used for the convenience of model discretization.

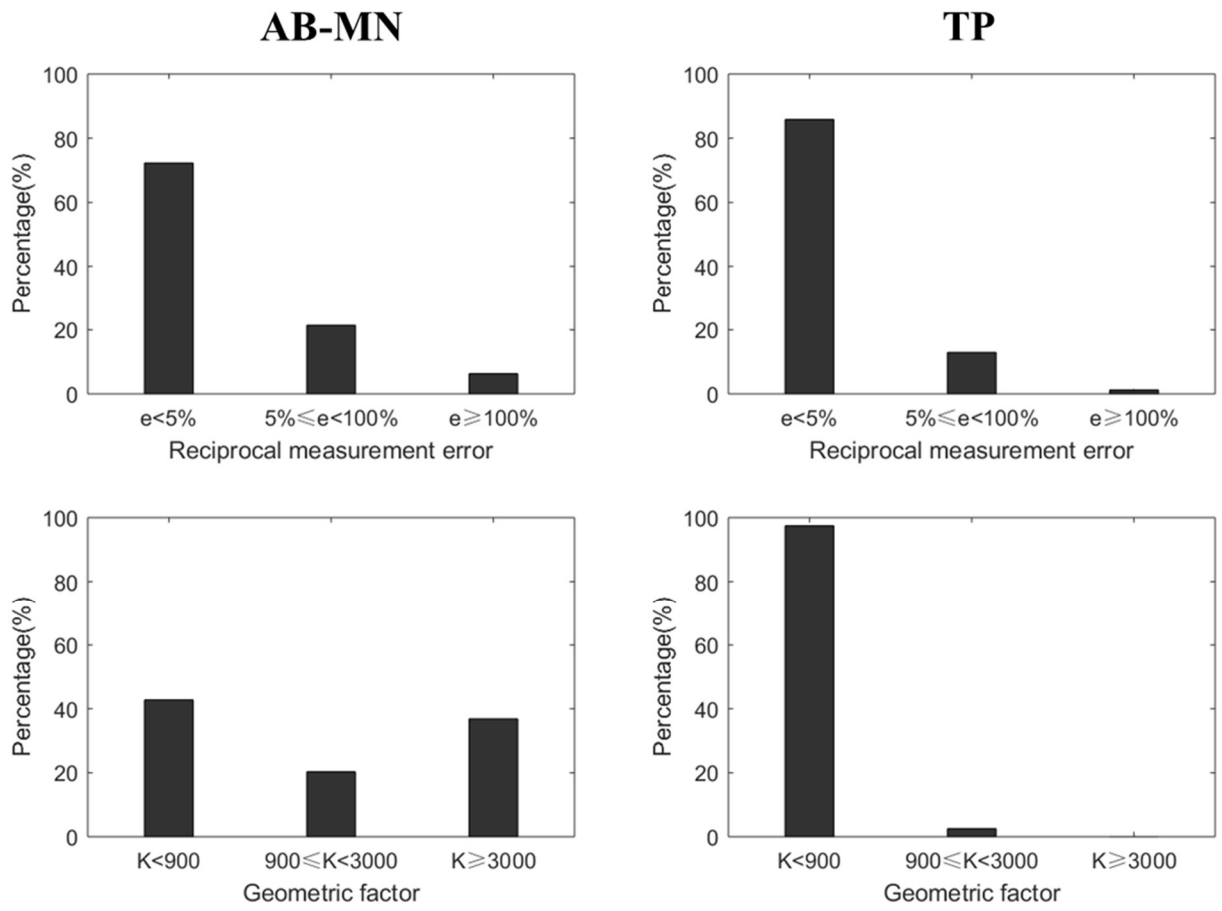

Figure 11: Statistics of reciprocal measurement error and geometric factor for AB-MN and TP arrays

The inversion of field data was carried out using RES2DINV software with the smoothness constraint inversion method and the results of different arrays and inversion models are shown in Figure 12. For the inverted resistivity sections, an apparent low resistivity layer near the depth of 8m is found in the results of AB-MN and NOPTs. However, the low resistivity layer cannot be clearly detected in the result of TP array. This may be explained by the symmetric effect in TP array. The symmetric effect induced by TP array may increase the resistivity between the boreholes and decease the resistivity outside the boreholes. It is also clear in the result of TP array with

extended model that resistivity values tend to be symmetrical with respect to the boreholes. The results in Figure 12 can be compared with the in-hole data (shown in Figure 13) measured by dipole-dipole array with 1 m electrode spacing in each borehole. It can be seen from Figure 13 that the maximum apparent resistivity value at the bottom is less than 200 Ωm. However, in the results of confined model of AB-MN and NOPTs in Figure 12, regions of much higher resistivity (over 500 Ωm) appears at the bottom as a result of incorrect boundary condition. Furthermore, apparent resistivity values at 8 m depth in Figure 13 range from 50 to 100 Ωm, agreeing better with all the inverted resistivity of NOPT arrays. This further verifies that the NOPT array shows better spatial resolution than the AB-MN array. The results of ratio 1:2 and 1:4 have a better resolution than ratio 1:1 because more TP data was included. The last two apparent resistivity values at the bottom of the left borehole are around 100 Ωm, which is apparently higher than the low apparent resistivity about 50 Ωm at the depth near 8m. This implies that there should be a relatively high resistivity body between these two depths. In this regard, the result of NOPT with ratio 1:2 (AB-MN:TP) seems more consistent with in-hole measurements than ratio 1:4. The ratio 1:2 seems to be a good compromise between resolution enhancement and symmetric effect suppression, supporting the suggestion of using ratio 1:2 in the nominal NOPT array. The relatively lower resistivity near 8 m depth is considered the residual effect of the low resistivity agents injected at depths between 5m and 10m using the double packer injection (DPI) method. Overall, following our proposed procedure, clearer structure and more accurate resistivity values were obtained by the NOPT array with extended inversion model.

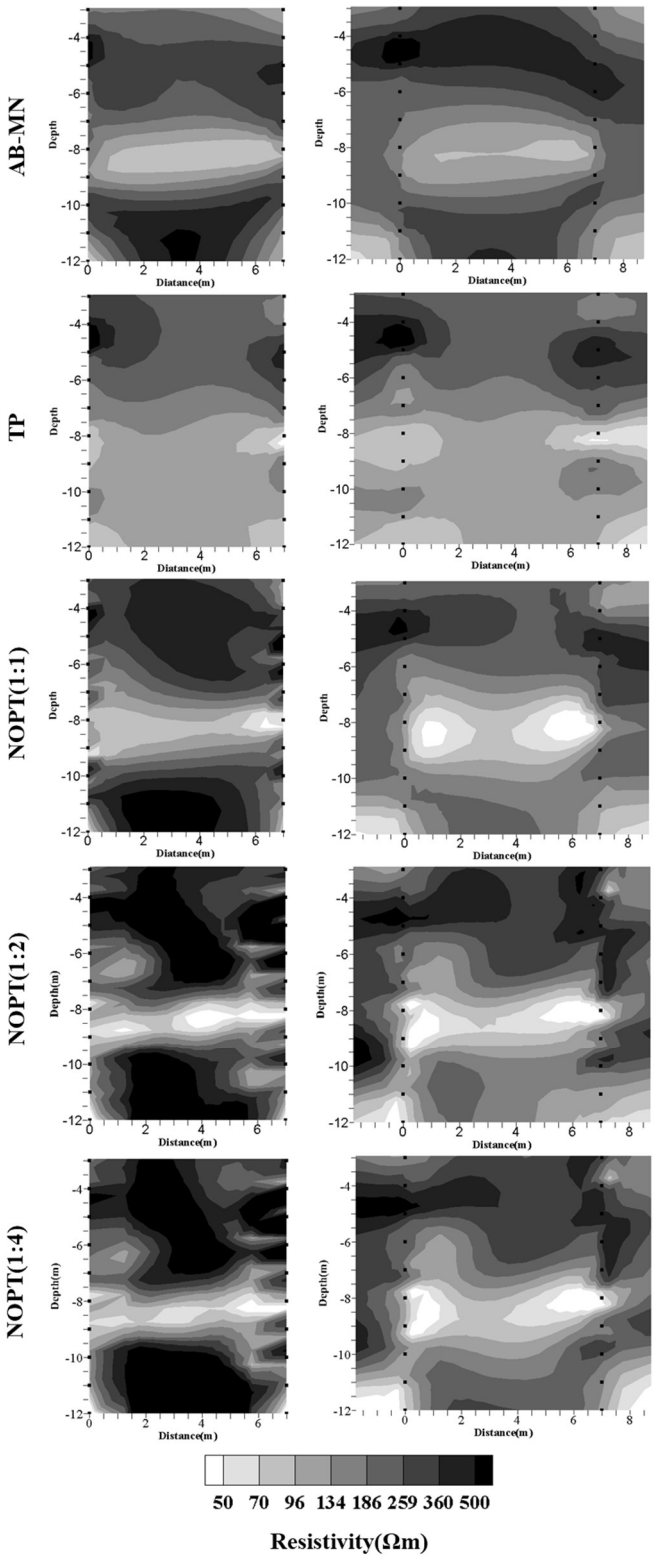

Figure 12: Inversion results of the field example with different arrays and inversion models

1

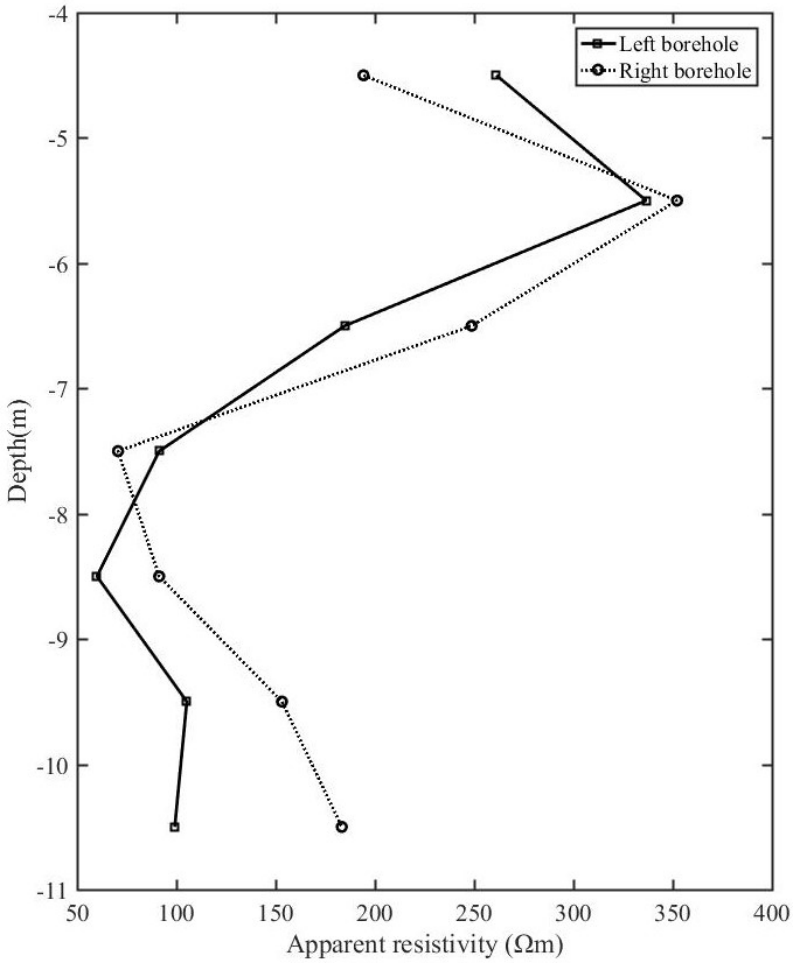

Figure 13: In-hole apparent resistivity profiles measured by dipole-dipole array with 1 m electrode spacing

6. Conclusions and suggestions

In this study, influence of outside anomaly in the CHERT method was investigated in the commonly used two-hole layout. The symmetric effect together with the effect of inversion range were investigated numerically in terms of different arrays and extension models. It was found that incorrect boundary condition in the CHERT data inversion may produce significantly anomalous results and aggravate the symmetric effect. By properly extending the inversion model, the results become much more reasonable. The symmetric effect does exist in the results of arrays when there are current pole and potential pole in a borehole concurrently, such as BB and TP arrays. AB-MN

array can produce results without symmetric anomalies; however, this type of array tends to have lower spatial resolution and the measured data is more sensitive to noise. It was found in the numerical results that properly combining arrays (i.e., AB-MN and TP) of different characteristics (sensitivity pattern and geometric factor) and extending the inversion model are more suitable and reasonable for CHERT data measurement and inversion.

For general CHERT surveys in practice, a general suggestion on the model extend ratio was given based on sensitivity analyses with different CHERT layout. Extended distance on each side should be about 0.25 times the borehole depth. Given the distinct characteristics of AB-MN and TP arrays in model resolution and symmetric effect, the recommended CHERT survey is the combination of AB-MN and TP arrays. When doing so, arrays with geometric factor greater than about 1000 should be excluded first and the data combination with 1:2 (AB-MN:TP) ratio is recommended as a general or nominal optimized array (NOPT). It is inevitable that the best data ratio will be model dependent. Nevertheless, a ratio about 1:2 is shown to provide sufficient AB-MN data to suppress the unwanted symmetric effect in the numerical studies and field example. It is possible to further lower the ratio from the 1:2 dataset if so desired for cases where symmetric effect is not a concern (e.g., the resistivity is quite uniform in horizontal direction). In the numerical results, the performance of the proposed NOPT array is similar to the OPT array proposed by Bellmunt et al. (2016) for the specific plume migration problem. However, NOPT array is a more general approach of array selection having advantages of better data quality control and easy implementation independent of resistivity model and cross-hole layout. A field example is presented to validate our proposed method and findings. The inversion shows better results and agreement with in-hole apparent resistivity data when using NOPT array and extended inversion

model. How to reduce total data amount or utilize data reconstruction to speed up data acquisition time for dynamic monitoring needs further studies.

7. Acknowledgment

This work was supported by a research program of Taiwan's Environmental Protection Administration. We sincerely thank the two anonymous reviewers for their helpful comments on our original manuscript.

8. References

AGI (Advanced Geosciences, Inc.), 2014. Instruction Manual for EarthImager 2D Version 2.4. 2 Resistivity and IP Inversion Software.

Bellmunt, F., Marcuello, A., Ledo, J. and Queralt, P., 2016. Capability of cross-hole electrical configurations for monitoring rapid plume migration experiments. *Journal of Applied Geophysics*, *124*, pp.73-82.

Brunet, P., Clément, R. and Bouvier, C., 2010. Monitoring soil water content and deficit using Electrical Resistivity Tomography (ERT)–A case study in the Cevennes area, France. *Journal of Hydrology*, *380*(1-2), pp.146-153.

Chambers, J.E., Kuras, O., Meldrum, P.I., Ogilvy, R.D. and Hollands, J., 2006. Electrical resistivity tomography applied to geologic, hydrogeologic, and engineering investigations at a former waste-disposal site. *Geophysics*, *71*(6), pp.B231-B239.

Chambers, J.E., Wilkinson, P.B., Wealthall, G.P., Loke, M.H., Dearden, R., Wilson, R., Allen, D. and Ogilvy, R.D., 2010. Hydrogeophysical imaging of deposit heterogeneity and

groundwater chemistry changes during DNAPL source zone bioremediation. *Journal of contaminant hydrology*, *118*(1-2), pp.43-61.

COMSOL Multiphysics 5.2, 2015, Geoelectrics – Forward problem and sensitivity https://www.comsol.com/model/a-geoelectrical-forward-problem-9636

Coscia, I., Greenhalgh, S.A., Linde, N., Doetsch, J., Marescot, L., Günther, T., Vogt, T. and Green, A.G., 2011. 3D crosshole ERT for aquifer characterization and monitoring of infiltrating river water. *Geophysics*, *76*(2), pp.G49-G59.

Coscia, I., Linde, N., Greenhalgh, S., Vogt, T. and Green, A., 2012. Estimating traveltimes and groundwater flow patterns using 3D time-lapse crosshole ERT imaging of electrical resistivity fluctuations induced by infiltrating river water. *Geophysics*, *77*(4), pp.E239-E250.

Daily, W. and Owen, E., 1991. Cross-borehole resistivity tomography. *Geophysics*, *56*(8), pp.1228-1235.

Friedel, S., 2003. Resolution, stability and efficiency of resistivity tomography estimated from a generalized inverse approach. *Geophysical Journal International*, *153*(2), pp.305-316.

Goes, B.J.M. and Meekes, J.A.C., 2004. An effective electrode configuration for the detection of DNAPLs with electrical resistivity tomography. *Journal of Environmental & Engineering Geophysics*, *9*(3), pp.127-141.

Guo, K., Milkreit, B. and Qian, W., 2014. Geometry factor for near surface borehole resistivity surveys: a key to accurate imaging and monitoring. *GeoConvention 2014*.

Ha, H.S., Kim, D.S. and Park, I.J., 2010. Application of electrical resistivity techniques to detect weak and fracture zones during underground construction. *Environmental Earth Sciences*, *60*(4), pp.723-731.

Hagrey, S.A., 2012. 2D optimized electrode arrays for borehole resistivity tomography and CO 2 sequestration modelling. *Pure and Applied Geophysics*, *169*(7), pp.1283-1292.

LaBrecque, D.J., Ramirez, A.L., Daily, W.D., Binley, A.M. and Schima, S.A., 1996. ERT monitoring of environmental remediation processes. *Measurement Science and Technology*, *7*(3), p.375.

Leontarakis, K. and Apostolopoulos, G.V., 2012. Laboratory study of the cross-hole resistivity tomography: the model stacking (MOST) technique. *Journal of Applied Geophysics*, *80*, pp.67-82.

Loke, M.H., Acworth, I. and Dahlin, T., 2003. A comparison of smooth and blocky inversion methods in 2D electrical imaging surveys. *Exploration Geophysics*, *34*(3), pp.182-187.

Loke, M.H., Wilkinson, P.B. and Chambers, J.E., 2010. Fast computation of optimized electrode arrays for 2D resistivity surveys. *Computers & Geosciences*, *36*(11), pp.1414-1426.

Loke, M.H., Wilkinson, P.B., Chambers, J.E. and Strutt, M., 2014. Optimized arrays for 2D cross-borehole electrical tomography surveys. *Geophysical Prospecting*, *62*(1), pp.172-189.

Loke, M.H., 2016. Tutorial: 2-D and 3-D electrical imaging surveys.

Nimmer, R.E., Osiensky, J.L., Binley, A.M. and Williams, B.C., 2008. Three-dimensional effects causing artifacts in two-dimensional, cross-borehole, electrical imaging. *Journal of Hydrology*, *359*(1-2), pp.59-70.

Oldenburg, D.W. and Li, Y., 1999. Estimating depth of investigation in dc resistivity and IP surveys. *Geophysics*, *64*(2), pp.403-416.

Park, S.K. and Van, G.P., 1991. Inversion of pole-pole data for 3-D resistivity structure beneath arrays of electrodes. *Geophysics*, *56*(7), pp.951-960.

Perri, M.T., Cassiani, G., Gervasio, I., Deiana, R. and Binley, A., 2012. A saline tracer test monitored via both surface and cross-borehole electrical resistivity tomography: Comparison of time-lapse results. *Journal of Applied Geophysics*, *79*, pp.6-16.

Roy, A. and Apparao, A., 1971. Depth of investigation in direct current methods. *Geophysics*, *36*(5), pp.943-959.

Rücker, C. and Günther, T., 2011. The simulation of finite ERT electrodes using the complete electrode model. *Geophysics*, *76*(4), pp.F227-F238.

Rücker, C., Günther, T. and Spitzer, K., 2006. Three-dimensional modelling and inversion of dc resistivity data incorporating topography—I. Modelling. *Geophysical Journal International*, *166*(2), pp.495-505.

Saad, R., Nawawi, M.N.M. and Mohamad, E.T., 2012. Groundwater detection in alluvium using 2-D electrical resistivity tomography (ERT). *Electronic Journal of Geotechnical Engineering*, *17*, pp.369-376.

Shima, H., 1989. Effects on reconstructed images of surrounding resistivity structures in resistivity tomography. In *SEG Technical Program Expanded Abstracts 1989* (pp. 385-389). Society of Exploration Geophysicists.

Slater, L., Binley, A.M., Daily, W. and Johnson, R., 2000. Cross-hole electrical imaging of a controlled saline tracer injection. *Journal of applied geophysics*, *44*(2-3), pp.85-102.

Slater, L. and Binley, A., 2006. Synthetic and field-based electrical imaging of a zerovalent iron barrier: Implications for monitoring long-term barrier performance. *Geophysics*, *71*(5), pp.B129-B137.

Stummer, P., Maurer, H. and Green, A.G., 2004. Experimental design: Electrical resistivity data sets that provide optimum subsurface information. *Geophysics*, *69*(1), pp.120-139.

Tsokas, G.N., Tsourlos, P.I., Vargemezis, G. and Novack, M., 2008. Non-destructive electrical resistivity tomography for indoor investigation: the case of Kapnikarea Church in Athens. *Archaeological Prospection*, *15*(1), pp.47-61.

Tsourlos, P., Ogilvy, R., Papazachos, C. and Meldrum, P., 2011. Measurement and inversion schemes for single borehole-to-surface electrical resistivity tomography surveys. *Journal of Geophysics and Engineering*, *8*(4), pp.487-497.

Wagner, F.M., Günther, T., Schmidt-Hattenberger, C. and Maurer, H., 2015. Constructive optimization of electrode locations for target-focused resistivity monitoring. *Geophysics*, *80*(2), pp.E29-E40.

Wagner, F.M., Möller, M., Schmidt-Hattenberger, C., Kempka, T. and Maurer, H., 2013. Monitoring freshwater salinization in analog transport models by time-lapse electrical resistivity tomography. *Journal of applied Geophysics*, *89*, pp.84-95.

Wang, H. and Lin, C.P., 2018. Cause and countermeasures for the symmetric effect in borehole-to-surface electrical resistivity tomography. *Journal of Applied Geophysics*, *159*, pp.248-259.

Wilkinson, P.B., Chambers, J.E., Meldrum, P.I., Ogilvy, R.D. and Caunt, S., 2006a. Optimization of array configurations and panel combinations for the detection and imaging of abandoned mineshafts using 3D cross-hole electrical resistivity tomography. *Journal of Environmental & Engineering Geophysics*, *11*(3), pp.213-221.

Wilkinson, P.B., Meldrum, P.I., Chambers, J.E., Kuras, O. and Ogilvy, R.D., 2006b. Improved strategies for the automatic selection of optimized sets of electrical resistivity tomography measurement configurations. *Geophysical Journal International*, *167*(3), pp.1119-1126.

Wilson, S.R., Ingham, M. and McConchie, J.A., 2006. The applicability of earth resistivity methods for saline interface definition. *Journal of hydrology*, *316*(1-4), pp.301-312.

Yi, M.J., Kim, J.H. and Son, J.S., 2009. Borehole deviation effect in electrical resistivity tomography. *Geosciences Journal*, *13*(1), p.87.

Zhou, B. and Greenhalgh, S.A., 2000. Cross-hole resistivity tomography using different electrode configurations. *Geophysical prospecting*, *48*(5), pp.887-912.